

Democratizing AI: Open-source Scalable LLM Training on GPU-based Supercomputers

Siddharth Singh^{†,1}, Prajwal Singhanian[†], Aditya Ranjan[†], John Kirchenbauer[†], Jonas Geiping^{*}, Yuxin Wen[†], Neel Jain[†], Abhimanyu Hans[†], Manli Shu[†], Aditya Tomar[§], Tom Goldstein[†], Abhinav Bhatele^{†,2}

[†]Department of Computer Science, University of Maryland, College Park, USA

^{*}ELLIS Institute Tübingen, Max Planck Institute for Intelligent Systems, Tübingen, Germany

[§]Department of Electrical Engineering and Computer Sciences, University of California, Berkeley, USA

E-mail: ¹ssingh37@umd.edu, ²bhatele@cs.umd.edu

Abstract—Training and fine-tuning large language models (LLMs) with hundreds of billions to trillions of parameters requires tens of thousands of GPUs, and a highly scalable software stack. In this work, we present a novel four-dimensional hybrid parallel algorithm implemented in a highly scalable, portable, open-source framework called AxoNN. We describe several performance optimizations in AxoNN to improve matrix multiply kernel performance, overlap non-blocking collectives with computation, and performance modeling to choose performance optimal configurations. These have resulted in unprecedented scaling and peak flop/s (bf16) for training of GPT-style transformer models on Perlmutter (620.1 Petaflop/s), Frontier (1.381 Exaflop/s) and Alps (1.423 Exaflop/s).

While the abilities of LLMs improve with the number of trainable parameters, so do privacy and copyright risks caused by memorization of training data, which can cause disclosure of sensitive or private information at inference time. We highlight this side effect of scale through experiments that explore “catastrophic memorization,” where models are sufficiently large to memorize training data in a single pass, and present an approach to prevent it. As part of this study, we demonstrate fine-tuning of a 405-billion parameter LLM using AxoNN on Frontier.

Index Terms—parallel training, GPGPUs, collective communication, asynchrony, large language models

I. JUSTIFICATION FOR ACM GORDON BELL PRIZE

A novel four-dimensional hybrid parallel approach to scale neural network training to tens of thousands of AMD and NVIDIA GPUs. Time-to-solution for 80-billion parameter GPT-style transformer models was reduced by 56.0 \times , due to kernel tuning, aggressive overlap, and optimization of collective communication. Unprecedented performance of 1.423 Exaflop/s on 6,144 NVIDIA H100 GPUs, 1.381 Exaflop/s on 32,768 AMD MI250X GCDs, and 620.1 Petaflop/s on 4,096 NVIDIA A100 GPUs in half-precision (bf16).

II. PERFORMANCE ATTRIBUTES

Category of achievement	peak performance, scalability, time-to-solution
Type of method used	n/a
Results reported on the basis of	whole application including input
Precision reported	mixed-precision
System scale	results measured on full-scale system
Measurement mechanism	timers and FLOP count

III. OVERVIEW OF THE PROBLEM

The field of generative artificial intelligence (AI) has taken the world by storm. In particular, large language models (LLMs) and their chatbot interfaces have become ubiquitous, employed by students, researchers, and professionals in various fields on a daily basis. Modern generative AI models are built by training extremely large neural networks, which have been shown to generalize extremely effectively with increases in model size. This unprecedented scaling of neural network training has been enabled by the emergence of highly efficient GPUs, and the availability of open source training frameworks such as PyTorch, and TensorFlow.

Training large neural networks that do not fit on a single GPU with 40-96 GB of RAM requires partitioning the model across multiple GPUs and parallelizing the matrix-matrix multiplication operations, which are a significant fraction of the overall computation. Scalability and parallel efficiency of DNN training is impacted by several factors – sustained flop/s and scalability of parallel matrix multiplication, performance of collective communication operations over sub-communicators, and the degree of overlap of computation with non-blocking collectives. While classical parallel algorithms for matrix multiplication such as SUMMA and Cannon’s 2D Matrix Multiply exist, they lead to significant communication bottlenecks when training models with hundreds of billions of parameters on hundreds of GPUs. All of these factors make efficient parallelization of DNN training a formidable task.

In this work, we target the challenging research problem of training models with hundreds of billions of parameters on the fastest supercomputers with thousands of GPUs. Traditionally, training at such scales has been restricted to companies with large budgets and access to significant GPU resources. However, programs such as INCITE for access to DOE supercomputers, Frontier and Perlmutter, and recent access to Alps at CSCS have enabled our team to solve the research challenges in the area of parallel training, and innovate in the area of AI/ML, by training and fine-tuning LLMs.

There are several different challenges in ensuring scalability and a high fraction of peak flop/s for parallel training. First, we need to ensure that math libraries such as cuBLAS and

rocBLAS are highly performant for matrix multiplication on NVIDIA and AMD GPUs respectively. Second, we have to ensure that both intra-node and inter-node communication of data (activations, parameters, and gradients) is performant, and overlapped with computation as much as possible. Third, when running on large GPU partitions with hundreds to thousands of GPUs, the decomposition of work and its mapping to GPUs should be near-optimal, taking communication into account.

In order to overcome the challenges mentioned above, we have developed a four-dimensional (4D) hybrid parallel approach that combines a three-dimensional (3D) matrix multiplication algorithm with data parallelism to achieve high efficiency at large GPU counts. In addition, we have improved the performance of our implementation using several optimizations. First, we tune our matrix multiplication for each individual platform. Second, we aggressively overlap computation with non-blocking collectives used in different phases of training. Third, since the 4D algorithm requires arranging the GPUs in an allocated job partition into a 4D virtual grid, this results in several potential configurations, not all of which are performance optimal. Hence, we have developed a communication model for 4D hybrid algorithms that can predict high-performing configurations given a problem size and number of GPUs. We have implemented all of the aforementioned innovations in AxoNN [9], [10], our open source framework for large scale parallel deep learning.

We have benchmarked and optimized AxoNN on both NVIDIA and AMD GPU-based platforms, and we present results on Perlmutter at NERSC/LBL, Frontier at OLCF/ORNL, and Alps at CSCS. We use a range of neural network sizes with 5 billion to 320 billion parameters. AxoNN achieves an unprecedented performance of 620.1 Petaflop/s on 4,096 NVIDIA A100 GPUs, 1.381 Exaflop/s on 32,768 MI250X GCDs, and 1.423 Exaflop/s on 6,144 NVIDIA H100 GPUs in half-precision (bf16).

Access to a highly scalable training framework and large supercomputers have also enabled the AI researchers on our team to study the inner workings of LLMs at model sizes that are impossible to study otherwise. One such problem is studying whether LLMs memorize training data and regenerate it verbatim during inference. This has privacy risks when personally identifiable information (PII) is memorized, and legal/copyright risks when models reproduce verbatim copies of text without the necessary copyright and licensing information. We present a study that explores the relationship between model size and the memorization properties of LLMs, and demonstrate the impact of a solution to reduce memorization.

IV. STATE OF THE ART IN PARALLEL TRAINING

In this section, we present the state of the art in scaling parallel training of deep neural networks to large-scale HPC systems and data centers.

A. Methods for Parallel DNN Training

Deep neural network training is typically parallelized using one of three approaches – data parallelism, tensor parallelism,

or pipeline parallelism, or a hybrid approach that combines some of the above. In data parallelism, all GPUs are assigned a full copy of the neural network, and parallelism is achieved by sharding the input batch equally among the GPUs. The main drawback of data parallelism is that it requires the entire network to fit on a single GPU. To mitigate this, sharded data parallelism has been developed, which divides the network parameters across GPUs [11]–[13] and performs extra communication to gather them when needed.

Model parallelism is used to train DNNs that far exceed the memory capacity of a single GPU, and it can be further divided into two approaches – tensor parallelism [14] and pipeline parallelism [6], [15]. The former parallelizes the computation of each layer of the neural network across several GPUs, and is the focus of our work. In pipeline parallelism, entire layers are assigned to each GPU. A popular framework for parallel training is Shoeybi et al.’s Megatron-LM [14], which uses a tensor parallel algorithm to parallelize a pair of fully-connected layers.

Several frameworks combine multiple approaches to develop hybrid methods. Narayanan et al. [6] extend Megatron-LM to support hybrid parallelism by combining tensor, pipeline, and data parallelism. Rajbhandari et al. introduce a sharded data parallelism approach called ZeRO [11], which is combined with pipeline and tensor parallelism in Microsoft’s training framework, DeepSpeed [16], [17]. Megatron-DeepSpeed uses Megatron-LM’s tensor parallelism.

Several other frameworks that further optimize DNN training have been proposed in recent times. GPT-NeoX builds upon Megatron-LM and DeepSpeed for ease of usage [18]. Wahib et al. introduce KARMA, an out-of-core data parallelism framework, managing CPU-GPU data transfers to alleviate GPU memory constraints [2]. Zheng et al. propose Alpa for automating neural network parallelization, optimizing communication across GPUs [19]. Colossal-AI [20] offers a unified interface for distributed deep learning training.

B. Large-scale Studies of Training LLMs

We now present recent studies on training large language models on some of the largest GPU-based clusters. Meta trained Llama 2 [21] on 2000 NVIDIA A100 GPUs. Jain et al. [1] benchmark the training of a variant of T5-Large [22] on 1024 NVIDIA V100 GPUs using their proposed sub-graph parallelism technique within the LBANN framework [23]. Wahib et al. [2] use KARMA to benchmark a 17B parameter model on 2048 NVIDIA V100 GPUs and report a 1.35x training speedup compared to ZeRO [11]. Narayanan et al. present a weak scaling study of Megatron-LM’s pipeline parallelism, achieving 52% of the peak NVIDIA A100 flop/s when benchmarking the training of a 1000B parameter model on 3072 GPUs [6]. Shaden et al. [5] use Megatron-LM and DeepSpeed [16] to train a 530B parameter language model on the Selene supercomputer [24] using 4480 NVIDIA A100 GPUs. They achieved 113 Tflop/s per GPU with 3360 GPUs, equivalent to 36% of the peak performance. Ziheng et al. [7] introduce MegaScale, a production system for training

TABLE I

COMPARISON OF LARGE-SCALE LLM TRAINING STUDIES, COVERING DIVERSE FRAMEWORKS AND HARDWARE. FOR EACH STUDY, WE LIST THE LARGEST HARDWARE COUNTS USED, CORRESPONDING MODEL & BATCH SIZE, PERCENTAGE OF PEAK FLOP/S, AND ACTUAL SUSTAINED FLOP/S.

Study	Framework	Model Size	Batch Size	Hardware	Scale	% Peak	Petaflop/s
SUPER [1]	LBANN	3B*	0.5M*	NVIDIA V100	1,024 GPUs	-	-
KARMA [2]	KARMA	17B	2.0M*	NVIDIA V100	2,048 GPUs	-	-
FORGE [3]	GPT-NeoX	1.44B	16.8M	AMD MI250X	2,048 GCDs	~29% [†]	~112.6 [†]
Dash et al. [4]	Megatron-DeepSpeed	1000B	19.7M	AMD MI250X	3,072 GCDs	31.9% [‡]	188.0 [‡]
MT-NLG [5]	Megatron-DeepSpeed	530B	4.0M	NVIDIA A100	3,360 GPUs	36%	379.7
Narayanan et al. [6]	Megatron-LM	1000B	6.3M	NVIDIA A100	3,072 GPUs	52%	502.0
MegaScale [7]	MegaScale	175B	12.5M	NVIDIA A100	12,288 GPUs	55%	2166.3
Google [8]	Cloud TPU Multislice Training	32B	417M	TPUv5e	55,094 TPUs	44.67%	4480.0
This Work	AxoNN [9]	40B	16.8M	NVIDIA A100	4,096 GPUs	49%	620.1
		320B	16.8M	AMD MI250X	32,768 GCDs	22%	1381.0
		60B	16.8M	NVIDIA H100	6,144 GPUs	23%	1423.1

* Estimated from description in paper as exact number not mentioned

[†] Estimated from plots in the paper as exact numbers not mentioned

[‡] Calculated from flop/s at lower GPU/GCD count and weak scaling efficiency

LLMs at scale, achieving a 55.2% of the peak flop/s when benchmarking a 175B parameter model on 12,288 NVIDIA A100 GPUs.

With the emergence of AMD GPUs, several studies have focused on training large language models on AMD systems. Yin et al. [3] train FORGE, an open suite of large language models for scientific computing on Frontier [25]. In their work, the authors show scaling performance for training FORGE on up to 2048 AMD MI250X GPUs, achieving 28% of the peak flop/s. Dash et al. [4] analyze efficient distributed training strategies on Frontier for training large language models. They achieve 31.96% of peak when benchmarking the training of a 1T parameter model on 1024 MI250X GPUs.

Google conducted a study on large-scale training jobs for LLMs using over 50,000 TPUv5e chips [8]. The authors achieve 44.67% of the peak TPUv5e performance when benchmarking a 32B parameter model on 50,944 TPUv5e chips. Table I provides a summary of these studies, indicating the largest scale (in terms of the number of GPUs/GCDs/TPUs) used and the corresponding flop/s achieved. The last set of row in the table presents the results of this work using our open-source training framework, AxoNN. With the exception of MegaScale, AxoNN has been scaled to the largest number of NVIDIA GPUs. To the best of our knowledge, AxoNN is the first framework to run on up to 32,768 AMD MI250X GCDs to achieve a sustained flop/s performance of 1.381 Exaflop/s.

V. INNOVATIONS REALIZED

Training deep neural networks on a single GPU involves processing subsets of the data called batches through the layers of a DNN in the forward pass to compute a loss, computing the gradient of the loss in a backward pass via backpropagation, and updating the parameters (also called “weights”) in the optimizer step. These three steps are repeated iteratively until all batches have been consumed, and this entire training process is referred to as an epoch. We now describe our novel approach to scaling the computation in the steps

described above in the context of large multi-billion parameter neural networks on thousands of GPUs.

A. A Four-Dimensional Hybrid Parallel Approach

We have designed a hybrid parallel approach that combines data parallelism with three-dimensional (3D) parallelization of the matrix multiplication routines.

Data Parallelism: In order to use a hybrid approach that combines data with tensor parallelism, we organize the total number of GPUs, G , into a virtual 2D grid, $G_{\text{data}} \times G_{\text{tensor}}$. This results in G_{data} groups of G_{tensor} GPUs each. We use data parallelism across the G_{data} groups, and tensor parallelism within each group. Each G_{data} group collectively has a full copy of the neural network and is tasked to process a unique shard of the input batch. At the end of an input batch, all groups have to synchronize their weights by issuing all-reduces on their gradients after every batch (this is also referred to as an iteration).

3D Parallel Matrix Multiplication (3D PMM): Next, we use each GPU group, composed of G_{tensor} GPUs to parallelize the work within their copy of the neural network. This requires distributing the matrices, and parallelizing the computation within every layer of the neural network across several GPUs. Note that most of the computation in transformers is comprised of large matrix multiplications within fully connected (FC) layers. Hence, in this section, we will focus on parallelizing FC layers with a 3D PMM algorithm.

We now describe how a single layer is parallelized, and the same method is applied to all the layers in the neural network. Each FC layer computes one half-precision (fp16 or bf16) matrix multiplication (input activation, I multiplied by the layer’s weight matrix, W) in the forward pass and two half-precision matrix multiplications (MMs) in the backward pass ($\frac{\partial L}{\partial O} \times W^T$ and $I^T \times \frac{\partial L}{\partial O}$, where L is the training loss, and O is the output activation.) Thus, parallelizing an FC layer requires parallelizing these three MM operations across multiple GPUs.

We adapt Agarwal et al.’s 3D parallel matrix multiplication algorithm [26], for parallelizing our MMs. The 3D refers to organizing the workers (GPUs) in a three-dimensional virtual grid. So, we organize the G_{tensor} GPUs further into a virtual 3D grid of dimensions $G_x \times G_y \times G_z$ (Figure 1). We do 2D decompositions of both I and W into sub-blocks and map them to orthogonal planes of the 3D grid. In the figure below, I is distributed in the XZ plane, and copied in the Y dimension. W is distributed in the XY plane and copied along the Z dimension. Once each GPU has a unique sub-block of I and W , it can compute a portion of the O matrix, which can be aggregated across GPUs in the X direction using all-reduces.

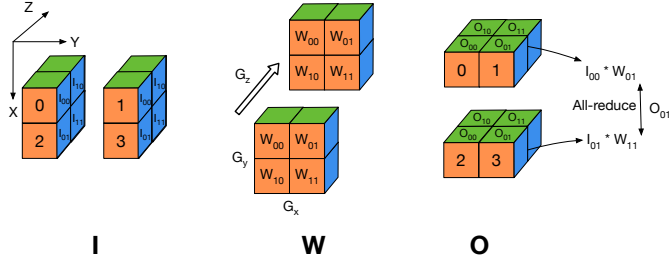


Fig. 1. Parallelization of a matrix multiply in an FC layer with Agarwal’s 3D parallel matrix multiplication algorithm [26] on eight GPUs organized in a $2 \times 2 \times 2$ topology. We use G_x , G_y , and G_z to refer to the number of GPUs along the three dimensions of the virtual grid topology.

We modify Agarwal’s algorithm to reduce memory consumption, and instead of making copies of W along the Z -axis, we further shard W along the Z -axis and denote these sub-shards as \hat{W} . Algorithm 1 presents the forward and backward pass operations on GPU $g_{i,j,k}$, and we can observe that the sharding of W results in all-gather operations before the local matrix multiplication on each GPU can proceed.

In the forward pass, after the local (to each GPU) matrix-multiply on line 3, we do an all-reduce to aggregate the output activations (line 4). In the backward pass, there are two matrix multiplies on lines 11 and 13, and corresponding all-reduce and reduce-scatter operations in lines 12 and 14 to get the data to the right GPUs.

Parallelizing an entire network: The approach of parallelizing a single layer in a deep neural network can be applied to all the layers individually. Let us consider a 2-layer neural network. If we use Algorithm 1 to parallelize each layer, the output O of the first layer would be the input to the other. However, notice in Figure 1 that O is distributed across the 3D virtual grid differently than the input I . So to ensure that the second layer can work with O , we would need to transpose its weight matrix – essentially dividing its rows across the X -axis and columns across the Y -axis. This transpose needs to be done once at the beginning of training. Hence, to parallelize a multi-layer neural network, we simply ‘transpose’ the weights of every other layer by swapping the roles of the X - and Y -tensor parallel groups.

Note that the 4D algorithm (data + 3D PMM) discussed in this section is a generalization of various state-of-the-art

Algorithm 1 Tensor parallel algorithm for $g_{i,j,k}$ in a $G_x \times G_y \times G_z$ grid. Communication operations highlighted in blue.

```

1: function TENSOR_PARALLEL_FORWARD_PASS( $I_{k,j}, \hat{W}_{j,i}$ )
2:    $W_{j,i} = \text{ALL-GATHER}_z(\hat{W}_{j,i})$ 
3:    $\hat{O}_{k,i} = I_{k,j} \times W_{j,i}$ 
4:    $O_{k,i} \leftarrow \text{ALL-REDUCE}_y(\hat{O}_{k,i})$ 
5:   // Cache  $I_{k,j}$  and  $W_{j,i}$  for the backward pass
6:   return  $O_{k,i}$ 
7: end function
8:
9: function TENSOR_PARALLEL_BACKWARD_PASS( $\frac{\partial L}{\partial O_{k,i}}$ )
10:  Retrieve  $I_{k,j}$  and  $W_{j,i}$  from cache
11:   $\frac{\partial \hat{L}}{\partial I_{k,j}} \leftarrow \frac{\partial L}{\partial O_{k,i}} \times W_{j,i}^\top$ 
12:   $\frac{\partial L}{\partial I_{k,j}} \leftarrow \text{ALL-REDUCE}_x(\frac{\partial \hat{L}}{\partial I_{k,j}})$ 
13:   $\frac{\partial L}{\partial \hat{W}_{j,i}} \leftarrow I_{k,j}^\top \times \frac{\partial L}{\partial O_{k,i}}$ 
14:   $\frac{\partial L}{\partial \hat{W}_{j,i}} \leftarrow \text{REDUCE-SCATTER}_z(\frac{\partial L}{\partial \hat{W}_{j,i}})$ 
15:  return  $\frac{\partial L}{\partial I_{k,j}}, \frac{\partial L}{\partial \hat{W}_{j,i}}$ 
16: end function

```

parallel deep learning algorithms. For example, if one were to employ only the Z axis of our PMM algorithm to parallelize training, it would reduce to Fully Sharded Data Parallelism (FSDP) [12] and ZeRO [11]. Similarly, if we employ the Z axis of 3D PMM and data parallelism simultaneously, then our algorithm reduces to Hybrid Sharded Data Parallelism [12] and ZeRO++ [27]. If we used the X axis of our 3D PMM algorithm along with the ‘transpose’ scheme discussed in the previous paragraph, our 4D algorithm reduces to Shoeybi et al.’s Megatron-LM [14]. Finally, when all four dimensions of our 4D algorithm are being used, this is similar to a hybrid scheme that combines data parallelism, FSDP, and two-dimensional tensor parallelism.

B. A Performance Model for Identifying Near-optimal Configurations

When assigned a job partition of G GPUs, we have to decide how to organize these GPUs into a 4D virtual grid, and how many GPUs to use for data parallelism versus the different dimensions of 3D parallel matrix multiplication. To automate the process of identifying the best performing configurations, we have developed a performance model that predicts the communication time of a configuration based on the neural network architecture, training hyperparameters, and network bandwidths. Using these predictions, we can create an ordered list of the best performing configurations as predicted by the model. We describe the inner-workings of this model below.

We primarily focus on modeling the performance of the collective operations in the code, namely all-reduces, reduce-scatters, and all-gathers. We first list the assumptions we make in our model:

- *Assumption-1:* The ring algorithm [28] is used for implementing the all-reduce, reduce-scatter, and all-gather collectives.
- *Assumption-2:* For collectives spanning more than one compute node, the ring is formed such that the number of messages crossing node boundaries is minimized.
- *Assumption-3:* The message sizes are large enough, and hence, message startup overheads can be ignored. In other words, if a process is sending a message of n bytes, then we assumed that the transmission time is simply $\frac{n}{\beta}$, where β is the available bandwidth between the two processes.
- *Assumption-4:* We only model the communication times and ignore the effects of any computation taking place on the GPUs.
- *Assumption-5:* We assume the same peer-to-peer bidirectional bandwidth, β_{inter} , between every pair of nodes.

We use the analytical formulations in Thakur et al. [28] and Rabenseifner [29] for modeling the performance of ring algorithm based collectives. Let $t_{\text{AG},z}$ denote the time spent in the all-gather across the Z -tensor parallel groups (line 2 of Algorithm 1). Similarly, we use $t_{\text{RS},z}$, $t_{\text{AR},y}$ and $t_{\text{AR},x}$ to refer to the time spent in the collectives in lines 14, 4, and 12 respectively. Similarly, we use $t_{\text{AR},\text{data}}$ for the time spent in the data parallel all-reduce. Then, we can model these times as follows,

$$t_{\text{AG},z} = \frac{1}{\beta} \times (G_z - 1) \times \frac{k \times n}{G_x \times G_y \times G_z} \quad (1)$$

$$t_{\text{RS},z} = \frac{1}{\beta} \times \left(\frac{G_z - 1}{G_z} \right) \times \frac{k \times n}{G_x \times G_y} \quad (2)$$

$$t_{\text{AR},y} = \frac{2}{\beta} \times \left(\frac{G_y - 1}{G_y} \right) \times \frac{m \times n}{G_z \times G_x} \quad (3)$$

$$t_{\text{AR},x} = \frac{2}{\beta} \times \left(\frac{G_x - 1}{G_x} \right) \times \frac{m \times k}{G_z \times G_y} \quad (4)$$

$$t_{\text{AR},\text{data}} = \frac{2}{\beta} \times \left(\frac{G_{\text{data}} - 1}{G_{\text{data}}} \right) \times \frac{k \times n}{G_x \times G_y \times G_z} \quad (5)$$

The total communication time for a single layer, t_{comm} is simply the sum of Equations 1 through 5:

$$t_{\text{comm}} = t_{\text{AG},z} + t_{\text{RS},z} + t_{\text{AR},y} + t_{\text{AR},x} + t_{\text{AR},\text{data}} \quad (6)$$

For layers with ‘transposed’ weight matrices as discussed at the end of Section V-A, we need to swap the values of G_x and G_y . And finally, to model the communication time for the entire network, we apply Equation 6 to all of its layers, and take a sum of the times.

In the equations derived above, we made a simplifying assumption that all collectives in our hybrid parallel method can achieve the highest peer-to-peer bandwidth, denoted by β . However, since several collectives are often in operation

at once, the actual bandwidth achieved for a collective operation among a group of GPUs depends on the placement of processes in our 4D virtual grid to the underlying hardware topology (nodes and network) [30]–[33]. For example, process groups that are contained entirely within a node can experience higher bandwidths than those containing GPUs on different nodes. Next, we model the specific bandwidths used in Equations 1 through 5.

To model the process group bandwidths, we begin by assuming a hierarchical organization of process groups: X -tensor parallelism (innermost), followed by Y -tensor parallelism, Z -tensor parallelism, and data parallelism (outermost). As a concrete example, if we have eight GPUs, and set $G_x = G_y = G_z = G_{\text{data}} = 2$, then the X -tensor parallel groups comprise of GPU pairs (0,1), (2,3), (4,5), and (6,7). Similarly, the Y -tensor parallel groups would comprise of GPU pairs (0,2), (1,3), (4,6), and (5,7), and so on.

Now let $\vec{G} = (G_x, G_y, G_z, G_{\text{data}})$ be the tuple of our configurable performance parameters, arranged in order of the assumed hierarchy. Let $\vec{\beta} = (\beta_x, \beta_y, \beta_z, \beta_{\text{data}})$ be the effective peer-to-peer bandwidths for collectives issued within these process groups. We use $\vec{\beta}_i$ and \vec{G}_i to represent the i^{th} elements of these tuples ($0 \leq i \leq 3$). Also, let G_{node} refer to the number of GPUs per node. Now let us model each β_i i.e. the bandwidth available to the GPUs in the process groups at the i^{th} level of the hierarchy.

Case 1: GPUs in the process group lie within a node – in our notation, this is the scenario when $\prod_{j=0}^i G_j \leq G_{\text{node}}$.

The bandwidth $\vec{\beta}_i$ is determined by two primary factors: (i) the size of the i^{th} process group, G_i , and (ii) the cumulative product of the sizes of all preceding process groups, $\prod_{j=0}^{i-1} G_j$. Given that the number of GPUs per node is typically small, the number of possible scenarios is also small. Therefore, we can profile the bandwidths for all potential configurations in advance and store this information in a database. Specifically, we generate all possible two-dimensional hierarchies of process groups (G_0, G_1) such that $G_0 \times G_1 \leq G_{\text{node}}$, and then perform simultaneous collectives within the outer process groups of size G_1 with a large message size of 1 GB. We record the achieved bandwidths for this tuple in our database. Then, for a given model, when we need the predicted bandwidths for the i^{th} process group, we retrieve the bandwidth recorded for the tuple $(G_0 = \prod_{j=0}^{i-1} G_j, G_1 = G_i)$.

Case 2: GPUs in the process group are on different nodes – in our notation, this is the scenario when $\prod_{j=0}^i G_j > G_{\text{node}}$.

For process groups spanning node boundaries, the approach of recording all possible configurations in a database is not feasible due to the vast number of potential scenarios, given the large number of possible sizes of these groups in a multi-GPU cluster. Therefore, we develop a simple analytical model for this scenario, which predicts the achieved bandwidths as a function of the inter-node bandwidths (β_{inter}), process group sizes (\vec{G}), and the number of GPUs per node (G_{node}).

First, let’s first explore two simple examples to build some intuition. In Figure 3, we demonstrate a scenario with a single

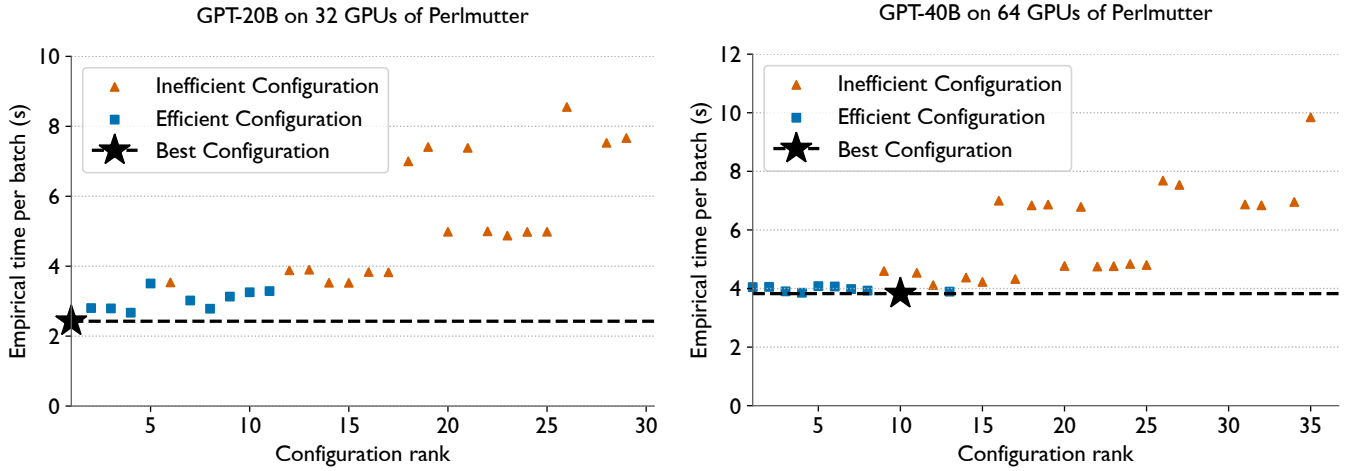


Fig. 2. Plots validating the performance model by comparing the observed time per batch and the rank ordered by the model for two neural networks: GPT-20B (left) and GPT-40B (right).

process group spanning eight GPUs on two nodes, with four GPUs on each node. In this case, the ring messages crossing node boundaries (i.e. the link between GPUs 1 and 4, and between GPUs 6 and 3) will be the communication bottleneck. Since we assumed β_{inter} to be the bidirectional bandwidth between node pairs, we can set $\beta_i = \beta_{\text{inter}}$.

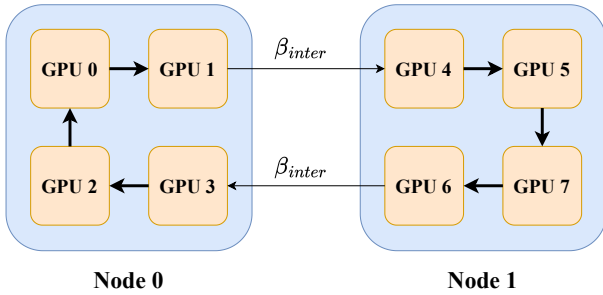


Fig. 3. Creation of a ring among eight GPUs on two nodes for a collective communication operation (all-reduce/reduce-scatter/all-gather).

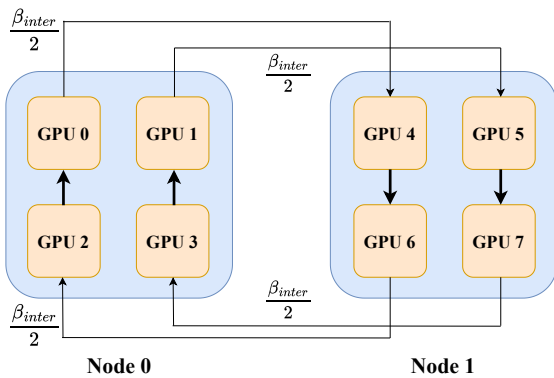


Fig. 4. Two rings among four GPUs each across two nodes for performing collective operations simultaneously.

Another possible scenario is when there are multiple si-

multaneous collectives taking place between two nodes. For example, consider Figure 4, wherein GPUs (0, 4, 6, 2) and GPUs (1, 5, 7, 3) are executing two independent collectives using the ring algorithm simultaneously. In this case, the available inter-node bandwidth will be shared between these two collectives and $\beta_i = \frac{\beta_{\text{inter}}}{2}$.

The first scenario occurs in the case when the process groups preceding the i^{th} process group in the hierarchy are of size one, i.e. $G_j = 1 \forall j < i$. Whereas the second scenario occurs in the case when at least one of these preceding process groups is of a size > 1 . In that case, we get multiple ring messages crossing node boundaries and the bandwidth gets distributed between the rings. However, note that the maximum reduction in the bandwidth is bounded by the total number of GPUs on each node, as there can't be more inter-node ring links than GPUs on a node. Equation 7 models all the scenarios to obtain the observed bandwidth:

$$\vec{\beta}_i = \frac{\beta_{\text{inter}}}{\min\left(G_{\text{node}}, \prod_{j=0}^{i-1} G_j\right)} \quad (7)$$

We use this bandwidth term in Equations 1 through 5 of our model. We use the model to create an ordered list of configurations, and then we can pick the top few configurations for actual experiments.

Validating the Performance Model: To validate the model, we collect the batch times for all possible configurations of the 4D virtual grid when training GPT-20B on 32 GPUs and GPT-40B on 64 GPUs of Perlmutter. Using the observed batch times, we label the ten fastest configurations as ‘efficient’ and the rest as ‘inefficient’. When creating the validation plots, we rank the configurations using the ordering provided by the performance model. Figure 2 shows the empirical batch times on the Y-axis and the rank output by the performance model on the X-axis. The fastest configurations should be in the lower left corner. We observe that nine out of the top ten configurations predicted by the performance model are indeed

‘efficient’ as per their observed batch times. This shows that the model is working very well in terms of identifying the fastest configurations.

C. Automated Tuning of BLAS Kernels

In deep neural networks, a significant portion of the computational workload is matrix multiplications kernels or “matmuls”, particularly in transformer models. These matmuls can be performed in one of three main modes based on whether the operands are transposed: NN, NT, and TN. Prior research has highlighted that NT and TN kernels are often less optimized than NN kernels in most BLAS libraries [34]. In our experiments, we found this discrepancy to be more pronounced when running transformers with large hidden sizes on the AMD MI250X GPUs of Frontier. For example, in the GPT-320B model (described in Table II), we observed that a matrix multiply defaulting to the TN mode in PyTorch achieved only 6% of the theoretical peak performance, whereas other matmuls reached 55% of the peak.

To address this issue, we implemented an automated tuning strategy in which, during the first batch, each matmul operation in the model is executed in all three modes (NN, NT, and TN) and timed. We then select the most efficient configuration for each operation, which is subsequently used for the remaining iterations. This tuning approach ensures that our deep learning framework, AxoNN, avoids the pitfalls of using suboptimal matmuls that could significantly degrade performance. For the aforementioned 320B model, our BLAS kernel tuning approach successfully switches the poorly performing TN matmul with a nearly $8\times$ faster NN matmul, thereby reducing the total time spent in computation from 30.1 seconds to 13.19s! Note that for other models used in Table II, the speedups attained via tuning are relatively modest (See Figure 7).

D. Overlapping Asynchronous Collectives with Computation

We use non-blocking collectives implemented in NCCL and RCCL on NVIDIA and AMD platforms respectively. This enables us to aggressively overlap the collective operations in AxoNN with computation, which can minimize communication overheads.

Overlapping All-reduces with Computation (OAR): In this performance optimization, we overlap the all-reduce across the X -tensor parallel groups in the backward pass (Line 12 of Algorithm 1) with the computation in Line 13. Once this computation has completed, we wait on the asynchronous all-reduce. Note that for layers with ‘transposed’ weight matrices, this communication happens across the Y -tensor parallel groups.

Overlapping Reduce-scatters with Computation (ORS): Next we overlap the reduce-scatters in the backward pass (line 14 of algorithm 1). The outputs of this reduce-scatter are the gradients of the loss w.r.t. the weights. These outputs are not needed until the backward pass is completed on all the layers of the neural network and we are ready to start issuing the all-reduces in the data parallel phase. Exploiting this, we issue

these reduce-scatters asynchronously and only wait on them once all layers have finished their backward pass. This allows us to overlap the reduce-scatter of one layer with the backward pass computations of the layers before it.

Overlapping All-gathers with Computation (OAG): Our next optimization overlaps the all-gather operations in the forward pass (line 2 of Algorithm 1) with computation. We observe that this all-gather operation does not depend on any intermediate outputs of the forward pass. Leveraging this, we preemptively enqueue the all-gather for the next layer while the computation for the current layer is ongoing. At the start of training, we generate a topological sort of the neural network computation graph to determine the sequence for performing the all-gathers. Subsequently, we execute them preemptively in this order.

Figure 5 shows the performance improvements from the three successive collective overlap optimizations (OAR: Overlap of all-reduces, ORS: Overlap of reduce-scatters, and OAG: Overlap of all-gathers). The baseline here refers to the scenario with no communication overlap. We also show the breakdown of the total time per batch into computation and communication. As we can see, the times spent in computation do not change significantly, however, the time spent in non-overlapped communication reduces with successive optimizations, leading to an overall speedup. For the 80B model in the figure, we see a performance improvement of 18.69% over the baseline on 8,192 GCDs of Frontier.

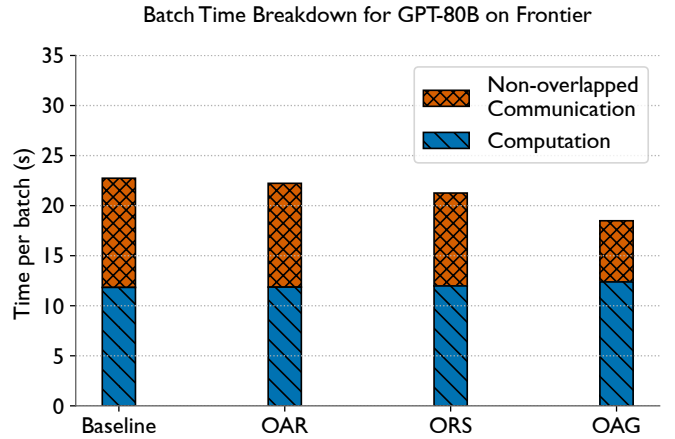


Fig. 5. The impact of overlapping non-blocking collectives with computation on the training times of different sized models on 8,192 GCDs of Frontier.

VI. HOW PERFORMANCE WAS MEASURED

All of our innovations are implemented in an open-source framework called AxoNN [9], which can be integrated easily as a backend in existing serial training codebases. This section provides details of the experimental setup for benchmarking training performance using AxoNN.

A. Applications: Model Architecture Details

We evaluate the effectiveness of our implementation by conducting experiments on a well-known neural network architec-

ture: Generative Pre-trained Transformer (GPT) [35]. The GPT architecture is a popular transformer architecture [36] that has been used to train several large language models [5], [35], [37], [38]. Table II presents the sizes of the different model architectures used in the experiments, and their important hyperparameters. Due to the extremely large activation memory requirements of training GPT models, we turn on activation checkpointing [39]. Additionally, we employ mixed precision (bf16/fp32) for all our training runs. We use bf16 since it has been shown to achieve the same performance and stability as fp32 [40], and it maintains the same range as fp32. This makes it a suitable choice over fp16, which has been known to be numerically unstable for LLM training.

TABLE II
ARCHITECTURAL DETAILS OF THE GPT-STYLE TRANSFORMERS [35]
USED IN THE PERFORMANCE EXPERIMENTS.

Model	# Parameters	# Layers	Hidden-Size	# Heads
GPT-5B	5B	24	4096	32
GPT-10B	10B	32	5120	40
GPT-20B	20B	32	7168	56
GPT-40B	40B	38	9216	72
GPT-60B	60B	56	9216	72
GPT-80B	80B	42	12288	96
GPT-160B	160B	84	12288	96
GPT-320B	320B	96	16384	128
GPT-640B	640B	192	16384	128

On Perlmutter, we use the sequential model training code from the Megatron-LM codebase [6], and parallelize it using AxoNN. However, on Frontier, we observed training instabilities with Megatron-LM, and switched to using LitGPT [41] for the model architectures on Frontier and Alps. We parallelized LitGPT also using our 4D implementation in AxoNN. We conduct weak scaling experiments with the GPT-3 models, ranging from 5 billion to 320 billion parameters. We also conduct strong scaling experiments on Frontier using the 80 billion and 640 billion parameter models to predict the time-to-solution for 2 trillion tokens.

B. Systems and Environments

Our experiments were conducted on three supercomputers, Perlmutter at NERSC/LBL, Frontier at OLCF/ORNL, and Alps at CSCS. Each node on Perlmutter is equipped with four NVIDIA A100 GPUs, each with a DRAM capacity of 40 GB. On Frontier, each node has four AMD Instinct MI250X GPUs each with a DRAM capacity of 128 GB. Each MI250X GPU is partitioned into two Graphic Compute Dies (GCDs) and each 64 GB GCD can be managed independently by a process. On Alps, each node has four GH200 Superchips, where each H100 GPU has a DRAM capacity of 96 GB. Nodes on all systems have four HPE Slingshot 11 NICs, with each NIC capable of bidirectional link speeds of 25 GB/s.

In our Perlmutter experiments, we use CUDA 11.7, NCCL 2.15.5, and PyTorch 1.13. On Frontier, we use PyTorch 2.2.1 with ROCm 5.7 and RCCL 2.18.6. On Alps, we use PyTorch 2.4.0 with CUDA 12.5.1 and NCCL 2.22.3. On all the systems,

we use the AWS OFI plugin (NCCL or RCCL) which enables us to use libfabric as the network provider on the Slingshot network, and provides high inter-node bandwidth. We want to note here that several runs on Perlmutter and Alps were done in a system-wide reservation, and even so, we noticed significant run-to-run performance variability. This was most likely due to network congestion [42] or file-system degradation [43] impacting performance.

C. Evaluation Metrics

In all our experiments, we run the training loop for ten iterations (batches), and report the average time per iteration (batch) for the last eight iterations to account for any performance variability due to initial warmup. We calculate half precision flop/s (often called “model flops”) using Narayanan et al.’s analytical formulation [6] for the number of floating point operations in a transformer model. We did a small experiment to verify that this formulation matches the total number of floating point operations measured by Nsight Compute, an empirical tool. We compare this number against the theoretical (vendor advertised) peak performance of each GPU (312 Tflop/s per GPU on Perlmutter, 191.5 Tflop/s per GCD on Frontier, 989 Tflop/s per GPU on Alps), and report the achieved percentage of peak as well as the total sustained bf16 flop/s.

Since the vendor advertised peak performance is often not practically achievable, we also ran a simple GEMM benchmark on 1 GPU/GCD of Perlmutter/Frontier to gather empirically observed peak flop/s. We invoked equivalent cuBLAS and rocBLAS kernel calls to multiply two bf16 square matrices with dimensions ranging from 1024 to 65536. On Perlmutter, the highest sustained flop/s for matrices of dimensions of 32768×32768 is 280 Tflop/s (90% of peak). On Frontier, the highest sustained flop/s is 125 Tflop/s on 1 GCD (65% of peak) for the same matrix dimensions. For Alps, we referred to a GH200 benchmark guide from NVIDIA that reported a sustained performance of 813 Tflop/s (82% of peak). These numbers show that the vendor advertised peak performance is almost always not achievable in practice. In our evaluation, we also report the % of peak empirical performance achieved by our implementation using the numbers mentioned above.

VII. PERFORMANCE RESULTS

We now discuss the results of our performance benchmarking experiments described in Section VI.

A. Weak Scaling Performance

We first present the weak scaling performance of AxoNN on Perlmutter, Frontier and Alps using GPT-style transformers as the application in Figure 6. We observe that on all three systems, AxoNN achieves near-ideal weak scaling up to 4096 GPUs/GCDs. This is particularly promising because most large-scale LLM training falls within this hardware range. When running the 60B model on 6144 H100 GPUs of Alps, we see a small reduction in efficiency – 76.5% compared to the performance on 1024 GPUs.

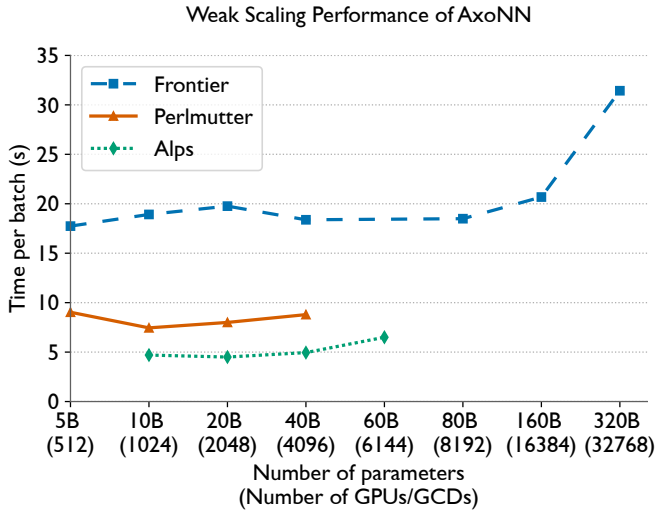


Fig. 6. Weak scaling performance (time per batch or iteration) of AxoNN on Frontier, Perlmutter, and Alps for models with 5 to 320 billion parameters.

Since Frontier has a significantly large number of GPUs than the other two platforms, we scaled AxoNN on Frontier to 32,768 GCDs. We see near perfect weak scaling up to 8,192 GCDs with a significantly high efficiency of 88.3% (compared to the performance on 512 GCDs). Although our weak performance drops at 16,384 GCDs, we are still able to sustain an efficiency of 79.02%. However, with rising overheads of communication, there is a notable decline in our performance on 32,768 GCDs, and a corresponding drop in efficiency to 53.5%.

We used timers to gather breakdowns of the time per batch into computation and non-overlapped communication to better understand the impact of the performance optimizations described in Section V. We present these results in Figure 7, for some model sizes running on 512–8,192 GCDs of Frontier. As a baseline, we use a configuration of AxoNN that corresponds to a hybrid of 1D tensor parallelism within node (similar to Megatron-LM [14]) and hybrid sharded data parallelism across nodes (similar to FSDP [12], [27]).

We observe that using the 3D parallel matrix multiplication and performance model to select the best configuration results in significant performance improvements of 13-45% over the baseline. Most of the improvement comes from a significant reduction in communication times. For the models in the plot, the improvements in the batch times due to our BLAS kernel tuning are relatively modest (2–4%). Finally, the improvement from our overlap optimizations is largest for the largest model in this series i.e. 80B on 8192 GCDs. In this case, we observe a 22% reduction in the batch times! This is expected because the overheads of communication tend to increase with scale and subsequently the benefits of our overlap optimizations become more pronounced.

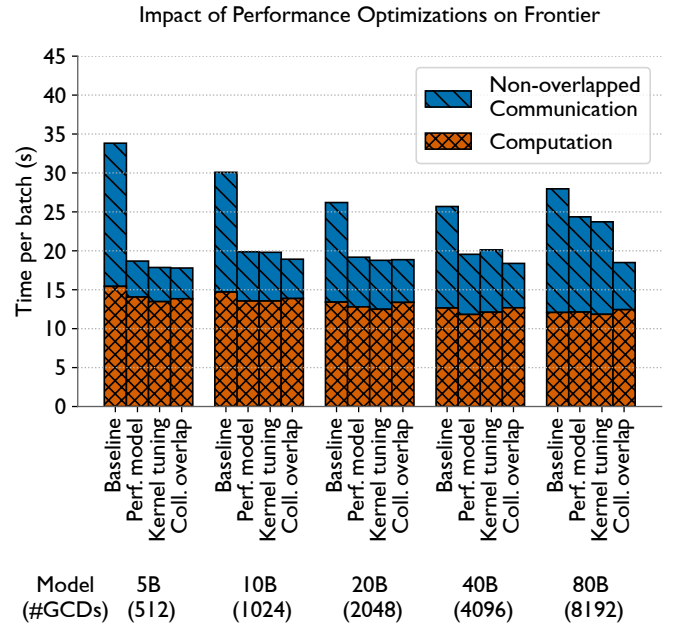


Fig. 7. The impact of our performance optimizations on weak scaling of GPT models. For the bars labeled “Perf model”, we use the best out of the top-10 configurations suggested by our communication model. For the bars labeled “Kernel Tuning” and “Comm Overlap”, we enable our matrix multiplication tuning and communication overlap optimizations.

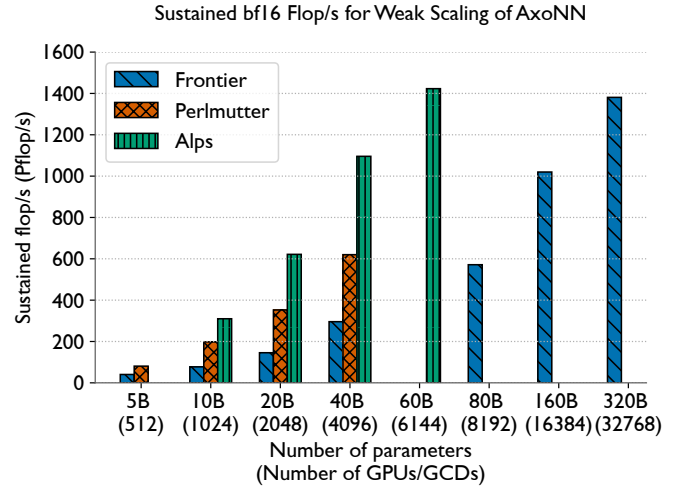


Fig. 8. Sustained flop/s on different platforms. The FLOP count is calculated analytically for all the matrix multiplication kernels in the code.

B. Sustained floating point operations per second (flop/s)

Next, we examine the floating-point operations per second (flop/s) achieved by AxoNN. In Figure 8, we present the total bf16 flop/s sustained by AxoNN in our weak scaling experiments on Perlmutter, Frontier and Alps. In Table III, we also show our sustained flop/s as a percentage of the vendor advertised and empirical obtained peak flop/s. As discussed in Section VI-B, we use 280 Tflop/s, 125 Tflop/s, and 813 Tflop/s as the empirical peak bf16 flop/s for an A100 GPU,

an MI250X GCD and an H100 GPU respectively.

On Perlmutter, we observe that AxoNN consistently sustains 50% or higher fraction of the advertised peak of 312 Tflop/s per GPU. As a result of our near perfect weak scaling, we observe that the sustained flop/s also increase linearly from 80.8 Pflop/s on 512 GPUs by nearly $8\times$ to 620.1 Pflop/s on 4096 GPUs. Since the advertised and empirical peak bf16 flop/s of an A100 GPU are close (312 vs. 280 Tflop/s), our % flop/s numbers are also in the same ball park.

TABLE III
SUSTAINED FLOP/S FOR WEAK SCALING ON PERLMUTTER, FRONTIER AND ALPS.

	# GPUs / GCDs	Model	Total Pfp/s	% of Advertised Peak	% of Empirical Peak
Perlmutter	512	5B	80.8	50.6	56.2
	1024	10B	197.8	61.9	68.8
	2048	20B	352.5	55.2	61.3
	4096	40B	620.1	48.5	53.9
Frontier	512	5B	40.4	41.1	63.3
	1024	10B	77.3	39.3	60.4
	2048	20B	145.7	37.0	57.0
	4096	40B	295.9	37.6	57.9
	8192	80B	571.4	36.3	56.0
	16384	160B	1019.9	32.4	49.9
	32768	320B	1381.0	22.0	33.8
Alps	1024	10B	310.0	30.6	37.3
	2048	20B	621.6	30.7	37.4
	4096	40B	1095.8	27.0	33.0
	6144	60B	1423.1	23.4	28.6

On Frontier, in the 512 to 4,096 GCD range, AxoNN achieves near-perfect weak scaling in terms of sustained flop/s which translates to a throughput of around 40% of the advertised peak performance. Notably, this is a significant improvement over Yin et al. [3] and Dash et al. [4] – they achieved a peak of only 30% in a similar range of GCDs, model sizes, and batch sizes on Frontier. AxoNN continues to scale well up to 8,192 GCDs, sustaining 36.3% of the peak and 571.4 Pflop/s in total. Beyond this scale, we start observing scaling inefficiencies. On 16,384 GCDs, we achieve 32.4% of the peak, which amounts to 1.02 Exaflop/s in total. Finally on 32,768 GCDs, our performance drops to 22% of the peak and a total flop/s of 1.381 Exaflop/s. In Section VI, we mentioned a significant difference between the advertised peak and the empirically measured peak on a single MI250X GCD (192 vs. 125 Tflop/s). As a result, there is a large difference between AxoNN’s flop/s expressed as a percentage of the advertised peak versus the empirical peak. For instance on 32,768 GCDs, these numbers are 22.0% and 33.8% respectively.

On Alps, we observe a similar trend as Perlmutter, with AxoNN consistently sustaining $\sim 30\%$ of the advertised peak up to 4096 GPUs. At 6144 GPUs, we see a slight drop to 23.42% of peak. At 6144 GPUs, we achieve our highest sustained flop/s of 1423.10 Pflop/s across all three machines.

C. Predicted Time-to-solution

The training of state-of-the-art large language models (LLMs) presents a significant computational challenge due

to two key factors. First, the models themselves are large, with current state-of-the-art models comprising hundreds of billions of trainable parameters. Second, LLMs are trained on massive and continually expanding text corpora, often containing trillions of tokens. In this section, we show how AxoNN can significantly reduce the time-to-solution of training such state-of-the-art LLMs on large text corpora. To demonstrate this, we pick the 80B and 640B parameter GPT models from Table II and collect the per iteration times at various GCD counts. We run the 80B model on 128 to 8,192 GCDs on Frontier, and the 640B model on 512 to 8,192 GCDs. We then extrapolate the batch times to estimate the time it would take to train these models to completion i.e. to ingest two trillion tokens. These time-to-solution results are presented in Figure 9. Note that both the model size and the number of tokens are representative of modern LLM training setups such as Meta’s Llama [21].

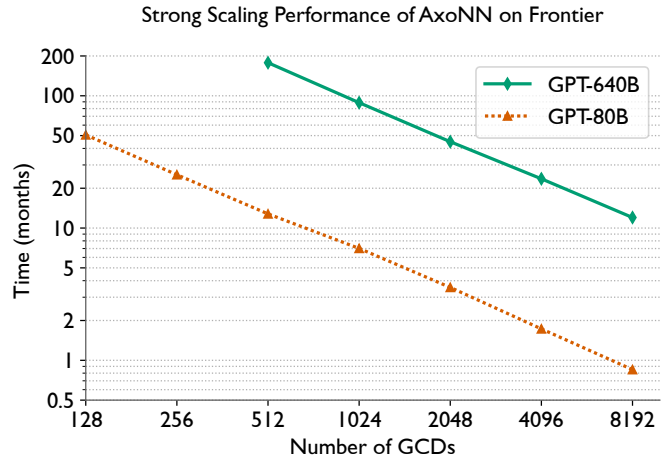


Fig. 9. Strong scaling showing expected time-to-solution on Frontier. Using the average time per iteration, we predict the training times for GPT-80B and GPT-640B on 2T tokens for various GCD counts.

As the plot shows, training an 80B model on 128 GCDs will take 50 months or more than four years. This emphasizes the critical role of large-scale parallelism in LLM training. As we scale to more GCDs, we see the expected time to solution drop almost linearly till 8,192 GCDs. Our estimate for the total training time of the 80B model on 8,192 GCDs is a much more reasonable 25.5 days. For the 640B model, even a much larger GCD count of 512 GCDs is impractical, with the estimated time-to-solution amounting to 14 years. However, on 8,192 GCDs, the estimated total training time is 15 months, which is an $11\times$ improvement. For both models, this amounts to a strong scaling efficiency of more than 90%. These experiments underscore AxoNN’s efficacy in significantly reducing the pre-training time for cutting-edge LLMs trained using massive datasets. By enabling faster training cycles on large scale multi-GPU clusters such as Frontier and Alps, AxoNN has the potential to accelerate the overall pace of LLM research and development.

VIII. IMPLICATIONS

A scalable training framework such as AxoNN and access to large supercomputers such as Frontier and Alps can enable studying properties of LLMs at scales that were impossible before. Below, we present a study on the behavior of memorization by large language models.

A. Memorization of Training Data by Large Language Models

A growing body of work has shown that language models memorize a portion of their training data and can reproduce this training data at inference time [44]. The ability of LLMs to reproduce training data has become a flashpoint for the AI community, as it poses major privacy and legal risks for commercial models [44]–[46].

It is thought that memorization is largely due to training data repetition, and it may be mitigated by dataset deduplication. Other factors such as data structure and model size may play a factor, but the issue is not well understood because public experiments have been constrained to smaller models (e.g. the popular Llama-2 7 billion parameter model [21]) with limited capacity and correspondingly small rates of memorization [44], [47]. As we observe below, the ability to memorize entire documents emerges only for large model sizes. Further, we hypothesize that models above a certain size threshold may exhibit *catastrophic memorization*, in which documents are memorized immediately in one single pass. When training a model above this size limit, even perfectly deduplicated datasets may still result in privacy and copyright leaks.

By creating scalable, user-friendly and portable access to model parallelism, AxoNN unlocks the potential for training and fine-tuning much larger models under commodity computing constraints using sequential LLM training codebases. This creates a scientific laboratory where large-model phenomena such as memorization can be publicly reproduced and studied. It also raises the ability of many practitioners to fine-tune large models on domain-specific data, expanding the need to understand memorization risks.

B. Experimental Setup: Training Llama models on Wikipedia

We design a targeted set of continued pre-training experiments to quantify the relationship between model size and memorization. We consider the Llama family of LLMs with publicly available pre-trained weights, and use the AxoNN infused LitGPT framework (introduced in Section VI-A) to parallelize the models. Our experiments start with pre-trained checkpoints for the TinyLlama-1B model [48], the 7B, 13B, and 70B parameter models in the Llama 2 family [21] and the 8B, 70B, and 405B parameter models from the recent Llama 3.1 release [49]. We train on English text data from Wikipedia with varying levels of repetition to quantify how memorization depends on model scale.

We train on English Wikipedia pages with 2048 tokens or more. The articles are randomly placed into one of four disjoint “buckets,” each with 200 articles. During training, the first three buckets are repeated for 1, 4, or 6 “epochs” (one pass over every page in the bucket) respectively. The fourth

bucket is a control group to measure baseline preexisting memorization from pre-training, and we do not perform any further training on the pages in the fourth bucket. After training is complete, we prompt the model with the beginning of each training sequence, and let the model write the last 50 tokens. We consider a sequence memorized if the model perfectly reproduces the correct 50 tokens.

We train the 1B, 7B, and 8B models on eight GCDs of Frontier using 8-way Z -tensor parallelism (i.e. $G_z = 8$), the 13B model using 16 GCDs, the 70B models using 64 GCDs, and the 405B model using 128 GCDs, each with a corresponding level of Z -tensor parallelism. The total batch size is fixed at 128 samples for all model sizes. In the case of smaller models, lower level of tensor parallelism is needed, so data parallelism is used to utilize the remaining GPUs. We warm up each model for 50 steps, increasing the learning rate to 3×10^{-4} on the non-bucketed Wikipedia pages, and then inject the three buckets of target data over the next 50 steps of training while decaying the learning rate to 3×10^{-5} . We report memorization for each bucket separately, and also for the held-out (“0 Ep”) control bucket.

C. Results: Catastrophic Memorization as a Function of Model Size

Figure 10 shows the impact of parameter count and number of epochs on exact memorization under otherwise identical conditions. At the 1B-13B scale (left plot), training for up to six epochs causes memorization of less than 1% of the 200 documents on average. However, we observe that the 70B models and the 405B model are capable of significant memorization (right plot). After just six passes over the data, the 70B Llama 2 and 70B Llama 3.1 models memorize 47% and 67% of documents on average respectively. Furthermore, we observe catastrophic memorization behavior starting at the 70B scale; roughly 5% of documents are memorized in just one single pass.

Moving to the 405B scale, we make several surprising observations. This model had already memorized over 10% of the control documents (see the bars labeled “0 Ep”) before our experiment even began, showing that the ability to memorize and retain documents during pre-training has emerged at this scale. While Wikipedia pages were certainly included in the training corpus of the Llama 3.1 series of models, only this largest model in the family exhibits such non-trivial levels of memorization without further continued training. Counterintuitively, we note that the rate of memorization of the 405B model during continued training was slower than that of the 70B model. This is likely because we used one set of hyperparameters for all models, and extreme scales likely require different hyperparameters for optimal learning.

D. Results: Goldfish Loss Stops Memorization in its Tracks

Observing extreme levels of memorization for models at the 70B parameter scale and above, we deploy a recently proposed technique for mitigating memorization in large language models. Language model training minimizes the expected cross-

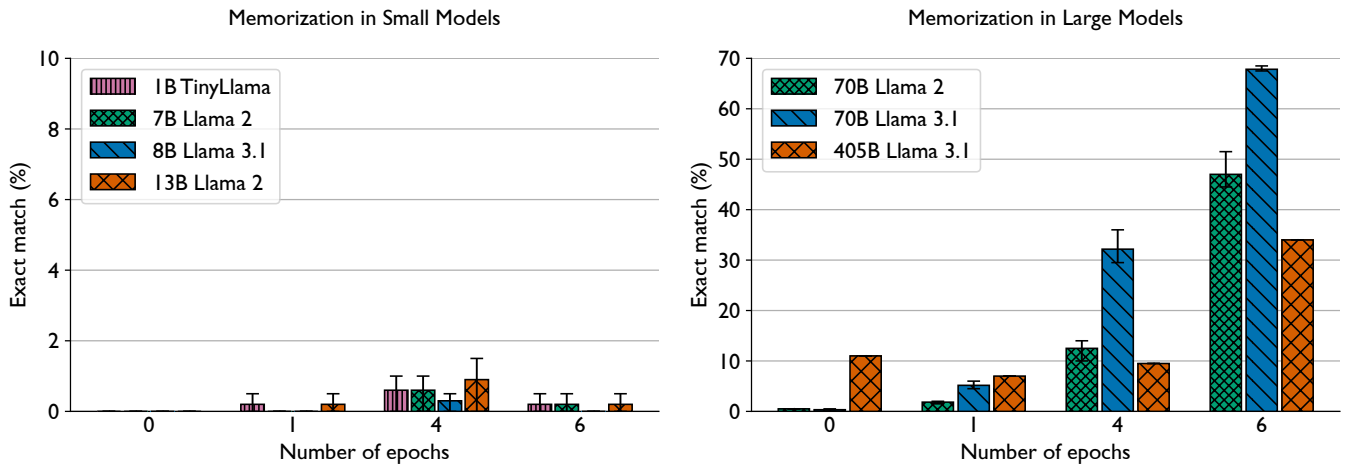


Fig. 10. Memorization as a function of parameter count and epochs (repetitions of the training data). For each model size, we show the “Exact Match” rate at which the model correctly reproduces the last 50 tokens of articles after being trained on them for various numbers of epochs. **(Left)** Memorization is difficult to observe for small models. **(Right)** The ability to efficiently memorize emerges at larger models scales. We see that a 70B model is even capable of *catastrophic memorization*, as it memorized entire documents after seeing them just once. For models with parameter counts in the 1B-13B range, we report the average over five trials, for 70B, we report the average over three trials, and for 405B we report a single trial. Error bars depict the min and max observed scores.

entropy between the language model’s next-token distribution and the true tokens as they appear in the training corpus. The *Goldfish Loss* [50] technique introduces a mask such that some tokens in any given training sequence are randomly omitted from the loss computation. The model cannot memorize the masked tokens, and must “guess” them when trying to reproduce a training sequence at inference time, making it very unlikely that long sequences can be exactly reproduced.

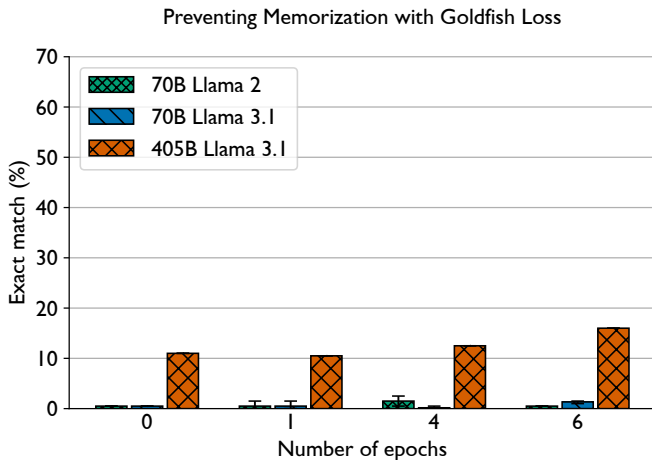


Fig. 11. The impact of applying Goldfish Loss during training to mitigate memorization in large models. The Exact Match rate reduces to levels comparable to the control data.

Figure 11 shows the results of re-running our training experiments with Goldfish Loss activated (using Goldfish parameters $k=2$, $h=13$). Even after continued training, memorization now reduces to levels comparable to the control data (0 Ep). We do observe a small increase in memorization as the 405B model trains, likely because the model has already memorized

the masked tokens from when it was pre-trained on Wikipedia. However, as we can see, the reduction in memorization when using the Goldfish Loss is significant, both for the 70B models and the 405B model.

ACKNOWLEDGMENT

A large number of people helped us in securing access and allocations at different supercomputing sites, and/or with improving the performance of our framework, and we wish to thank each one of them. For compute time allocations and reservations: Richard Gerber and Rebecca Hartman-Baker at NERSC/LBL; Bronson Messer and Phil Roth at ORNL; Maria-Grazia Giuffreda at CSCS; and Jack Wells at NVIDIA. For help with runs and software stack issues: Kevin Gott and Peter Harrington at NERSC/LBL; Jens Glaser and Michael Sandoval at ORNL; Fabian Bösch, Theofilos Manitaras, Henrique Mendonça, and Fawzi Mohamed at CSCS; Nicholas Malaya and Alessandro Fanfarillo at AMD; Tom Gibbs, and Josh Romero at NVIDIA; Mark Stock and Mengshiou Wu at HPE; and others working behind the scenes.

This material is based upon work supported in part by the ONR and OFOSR MURI programs, and the National Science Foundation (IIS-2229885 & IIS-2212182). An award for computer time was provided by the U.S. Department of Energy’s (DOE) Innovative and Novel Computational Impact on Theory and Experiment (INCITE) Program. This research used resources of: (1) the Oak Ridge Leadership Computing Facility at the Oak Ridge National Laboratory, which is supported by the Office of Science of the U.S. DOE under Contract No. DE-AC05-00OR22725, (2) the National Energy Research Scientific Computing Center (NERSC), a DOE Office of Science User Facility using NERSC awards DDR-ERCAP0029894 and DDR-ERCAP0029890, and (3) the Swiss National Supercomputing Centre (CSCS).

REFERENCES

- [1] A. Jain, T. Moon, T. Benson, H. Subramoni, S. A. Jacobs, D. K. Panda, and B. V. Essen, "Super: Sub-graph parallelism for transformers," in *2021 IEEE International Parallel and Distributed Processing Symposium (IPDPS)*, 2021, pp. 629–638.
- [2] M. Wahib, H. Zhang, T. T. Nguyen, A. Drozd, J. Domke, L. Zhang, R. Takano, and S. Matsuoka, "Scaling distributed deep learning workloads beyond the memory capacity with karma," in *Proceedings of the International Conference for High Performance Computing, Networking, Storage and Analysis*, ser. SC '20. IEEE Press, 2020.
- [3] J. Yin, S. Dash, F. Wang, and M. Shankar, "Forge: Pre-training open foundation models for science," in *Proceedings of the International Conference for High Performance Computing, Networking, Storage and Analysis*, ser. SC '23. New York, NY, USA: Association for Computing Machinery, 2023.
- [4] S. Dash, I. R. Lyngaas, J. Yin, X. Wang, R. Egele, J. A. Ellis, M. Maiterth, G. Cong, F. Wang, and P. Balaprakash, "Optimizing distributed training on frontier for large language models," in *ISC High Performance 2024 Research Paper Proceedings (39th International Conference)*, 2024, pp. 1–11.
- [5] S. Smith, M. Patwary, B. Norick, P. LeGresley, S. Rajbhandari, J. Casper, Z. Liu, S. Prabhume, G. Zerveas, V. Korthikanti, E. Zhang, R. Child, R. Y. Aminabadi, J. Bernauer, X. Song, M. Shoeybi, Y. He, M. Houston, S. Tiwary, and B. Catanzaro, "Using deepspeed and megatron to train megatron-turing nlg 530b, a large-scale generative language model," Tech. Rep., 2022.
- [6] D. Narayanan, M. Shoeybi, J. Casper, P. LeGresley, M. Patwary, V. Korthikanti, D. Vainbrand, P. Kashinkunti, J. Bernauer, B. Catanzaro, A. Phanishayee, and M. Zaharia, "Efficient large-scale language model training on GPU clusters," *CoRR*, vol. abs/2104.04473, 2021.
- [7] Z. Jiang, H. Lin, Y. Zhong, Q. Huang, Y. Chen, Z. Zhang, Y. Peng, X. Li, C. Xie, S. Nong, Y. Jia, S. He, H. Chen, Z. Bai, Q. Hou, S. Yan, D. Zhou, Y. Sheng, Z. Jiang, H. Xu, H. Wei, Z. Zhang, P. Nie, L. Zou, S. Zhao, L. Xiang, Z. Liu, Z. Li, X. Jia, J. Ye, X. Jin, and X. Liu, "MegaScale: Scaling large language model training to more than 10,000 GPUs," in *21st USENIX Symposium on Networked Systems Design and Implementation (NSDI 24)*. Santa Clara, CA: USENIX Association, Apr. 2024, pp. 745–760. [Online]. Available: <https://www.usenix.org/conference/nsdi24/presentation/jiang-ziheng>
- [8] Google, "Google cloud demonstrates the world's largest distributed training job for large language models across 50000+ tpu v5e chips," <https://cloud.google.com/blog/products/compute/the-worlds-largest-distributed-llm-training-job-on-tpu-v5e>.
- [9] S. Singh and A. Bhatele, "AxoNN: An asynchronous, message-driven parallel framework for extreme-scale deep learning," in *Proceedings of the IEEE International Parallel & Distributed Processing Symposium*, ser. IPDPS '22. IEEE Computer Society, May 2022.
- [10] —, "Exploiting sparsity in pruned neural networks to optimize large model training," in *2023 IEEE International Parallel and Distributed Processing Symposium (IPDPS)*. Los Alamitos, CA, USA: IEEE Computer Society, may 2023, pp. 245–255. [Online]. Available: <https://doi.ieeecomputersociety.org/10.1109/IPDPS54959.2023.00033>
- [11] S. Rajbhandari, J. Rasley, O. Ruwase, and Y. He, "Zero: Memory optimizations toward training trillion parameter models," in *Proceedings of the International Conference for High Performance Computing, Networking, Storage and Analysis*, ser. SC '20. IEEE Press, 2020.
- [12] Y. Zhao, A. Gu, R. Varma, L. Luo, C.-C. Huang, M. Xu, L. Wright, H. Shojanazeri, M. Ott, S. Shleifer, A. Desmaison, C. Balioglu, P. Damania, B. Nguyen, G. Chauhan, Y. Hao, A. Mathews, and S. Li, "Pytorch fsdp: Experiences on scaling fully sharded data parallel," *Proc. VLDB Endow.*, vol. 16, no. 12, p. 3848–3860, aug 2023.
- [13] G. Wang, H. Qin, S. A. Jacobs, X. Wu, C. Holmes, Z. Yao, S. Rajbhandari, O. Ruwase, F. Yan, L. Yang, and Y. He, "ZeRO++: Extremely efficient collective communication for large model training," in *The Twelfth International Conference on Learning Representations*, 2024. [Online]. Available: <https://openreview.net/forum?id=gx2BT0a9MQ>
- [14] M. Shoeybi, M. Patwary, R. Puri, P. LeGresley, J. Casper, and B. Catanzaro, "Megatron-lm: Training multi-billion parameter language models using model parallelism," Tech. Rep., 2020.
- [15] Y. Huang, Y. Cheng, A. Bapna, O. Firat, D. Chen, M. Chen, H. Lee, J. Ngiam, Q. V. Le, Y. Wu, and z. Chen, "GPipe: efficient training of giant neural networks using pipeline parallelism," in *Advances in Neural Information Processing Systems*, vol. 32. Curran Associates, Inc., 2019.
- [16] Microsoft, "DeepSpeed: Extreme-scale model training for everyone," <https://www.microsoft.com/en-us/research/blog/deepspeed-extreme-scale-model-training-for-everyone/>.
- [17] S. Singh, O. Ruwase, A. A. Awan, S. Rajbhandari, Y. He, and A. Bhatele, "A hybrid tensor-expert-data parallelism approach to optimize mixture-of-experts training," in *Proceedings of the 37th International Conference on Supercomputing*, ser. ICS '23. New York, NY, USA: Association for Computing Machinery, 2023, p. 203–214. [Online]. Available: <https://doi.org/10.1145/3577193.3593704>
- [18] A. Andonian *et al.*, "GPT-NeoX: Large Scale Autoregressive Language Modeling in PyTorch," 9 2023. [Online]. Available: <https://www.github.com/eleutherai/gpt-neox>
- [19] L. Zheng, Z. Li, H. Zhang, Y. Zhuang, Z. Chen, Y. Huang, Y. Wang, Y. Xu, D. Zhuo, J. E. Gonzalez, and I. Stoica, "Alpa: Automating inter- and intra-operator parallelism for distributed deep learning," *CoRR*, vol. abs/2201.12023, 2022.
- [20] S. Li, H. Liu, Z. Bian, J. Fang, H. Huang, Y. Liu, B. Wang, and Y. You, "Colossal-AI: a unified deep learning system for large-scale parallel training," in *Proceedings of the 52nd International Conference on Parallel Processing*, ser. ICPP '23. New York, NY, USA: Association for Computing Machinery, 2023, p. 766–775.
- [21] H. Touvron *et al.*, "Llama 2: Open foundation and fine-tuned chat models," Tech. Rep., 2023.
- [22] C. Raffel, N. Shazeer, A. Roberts, K. Lee, S. Narang, M. Matena, Y. Zhou, W. Li, and P. J. Liu, "Exploring the limits of transfer learning with a unified text-to-text transformer," 2019. [Online]. Available: <https://arxiv.org/abs/1910.10683>
- [23] B. V. Essen, H. Kim, R. A. Pearce, K. Boakye, and B. Chen, "LBANN: livermore big artificial neural network HPC toolkit," in *Proceedings of the Workshop on Machine Learning in High-Performance Computing Environments, MLHPC 2015, Austin, Texas, USA, November 15, 2015*. ACM, 2015, pp. 5:1–5:6.
- [24] "Nvidia selene supercomputer," <https://www.top500.org/system/179842/>.
- [25] S. Atchley *et al.*, "Frontier: Exploring exascale," in *Proceedings of the International Conference for High Performance Computing, Networking, Storage and Analysis*, ser. SC '23. New York, NY, USA: Association for Computing Machinery, 2023.
- [26] R. C. Agarwal, S. M. Balle, F. G. Gustavson, M. Joshi, and P. Palkar, "A three-dimensional approach to parallel matrix multiplication," *IBM Journal of Research and Development*, vol. 39, no. 5, pp. 575–582, 1995.
- [27] G. Wang, H. Qin, S. A. Jacobs, X. Wu, C. Holmes, Z. Yao, S. Rajbhandari, O. Ruwase, F. Yan, L. Yang, and Y. He, "ZeRO++: Extremely efficient collective communication for large model training," in *The Twelfth International Conference on Learning Representations*, 2024. [Online]. Available: <https://openreview.net/forum?id=gx2BT0a9MQ>
- [28] R. Thakur and W. D. Gropp, "Improving the performance of collective operations in mpich," in *Recent Advances in Parallel Virtual Machine and Message Passing Interface*, J. Dongarra, D. Laforenza, and S. Orlando, Eds. Berlin, Heidelberg: Springer Berlin Heidelberg, 2003, pp. 257–267.
- [29] R. Rabenseifner, "Optimization of collective reduction operations," in *Computational Science - ICCS 2004*, M. Bubak, G. D. van Albada, P. M. A. Sloot, and J. Dongarra, Eds. Berlin, Heidelberg: Springer Berlin Heidelberg, 2004, pp. 1–9.
- [30] E. Solomonik, A. Bhatele, and J. Demmel, "Improving communication performance in dense linear algebra via topology aware collectives," in *Proceedings of the International Conference for High Performance Computing, Networking, Storage and Analysis*, ser. SC '11. ACM, Nov. 2011, ILNL-CONF-491442. [Online]. Available: <http://doi.acm.org/10.1145/2063384.2063487>
- [31] A. Bhatele, T. Gambin, S. H. Langer, P.-T. Bremer, E. W. Draeger, B. Hamann, K. E. Isaacs, A. G. Landge, J. A. Levine, V. Pascucci, M. Schulz, and C. H. Still, "Mapping applications with collectives over sub-communicators on torus networks," in *Proceedings of the ACM/IEEE International Conference for High Performance Computing, Networking, Storage and Analysis*, ser. SC '12. IEEE Computer Society, Nov. 2012, ILNL-CONF-556491. [Online]. Available: <http://doi.ieeecomputersociety.org/10.1109/SC.2012.75>
- [32] A. Abdel-Gawad, M. Thottethodi, and A. Bhatele, "RAHTM: Routing-algorithm aware hierarchical task mapping," in *Proceedings of the*

- ACM/IEEE International Conference for High Performance Computing, Networking, Storage and Analysis*, ser. SC '14. IEEE Computer Society, Nov. 2014, ILNL-CONF-653568. [Online]. Available: <http://doi.ieeecomputersociety.org/10.1109/SC.2014.32>
- [33] A. Bhatele, N. Jain, K. E. Isaacs, R. Buch, T. Gamblin, S. H. Langer, and L. V. Kale, "Optimizing the performance of parallel applications on a 5D torus via task mapping," in *Proceedings of IEEE International Conference on High Performance Computing*, ser. HiPC '14. IEEE Computer Society, Dec. 2014, ILNL-CONF-655465. [Online]. Available: <http://doi.ieeecomputersociety.org/10.1109/HiPC.2014.7116706>
- [34] S. Shi, P. Xu, and X. Chu, "Supervised learning based algorithm selection for deep neural networks," in *2017 IEEE 23rd International Conference on Parallel and Distributed Systems (ICPADS)*, 2017, pp. 344–351.
- [35] T. B. Brown *et al.*, "Language models are few-shot learners," *CoRR*, vol. abs/2005.14165, 2020. [Online]. Available: <https://arxiv.org/abs/2005.14165>
- [36] A. Vaswani, N. Shazeer, N. Parmar, J. Uszkoreit, L. Jones, A. N. Gomez, L. Kaiser, and I. Polosukhin, "Attention is all you need," *CoRR*, vol. abs/1706.03762, 2017. [Online]. Available: <http://arxiv.org/abs/1706.03762>
- [37] BigScience, "Bigscience large open-science open-access multilingual language model," <https://huggingface.co/bigscience/bloom>, 2022.
- [38] A. Radford, J. Wu, R. Child, D. Luan, D. Amodei, and I. Sutskever, "Language models are unsupervised multitask learners," Tech. Rep., 2019.
- [39] T. Chen, B. Xu, C. Zhang, and C. Guestrin, "Training deep nets with sublinear memory cost," *CoRR*, vol. abs/1604.06174, 2016. [Online]. Available: <http://arxiv.org/abs/1604.06174>
- [40] D. D. Kalamkar, D. Mudigere, N. Mellempudi, D. Das, K. Banerjee, S. Avancha, D. T. Vooturi, N. Jammalamadaka, J. Huang, H. Yuen, J. Yang, J. Park, A. Heinecke, E. Georganas, S. Srinivasan, A. Kundu, M. Smelyanskiy, B. Kaul, and P. Dubey, "A study of BFLOAT16 for deep learning training," *CoRR*, vol. abs/1905.12322, 2019. [Online]. Available: <http://arxiv.org/abs/1905.12322>
- [41] Lightning AI, "Litgpt," <https://github.com/Lightning-AI/litgpt>, 2023.
- [42] H. Bhatia, N. Jain, A. Bhatele, Y. Livnat, J. Domke, V. Pascucci, and P.-T. Bremer, "Interactive investigation of traffic congestion on fat-tree networks using TreeScope," *Computer Graphics Forum*, vol. 37, no. 3, pp. 561–572, Jun. 2018.
- [43] M. Mubarak, P. Carns, J. Jenkins, J. Li, N. Jain, S. Snyder, R. B. Ross, C. D. Carothers, A. Bhatele, and K.-L. Ma, "Quantifying I/O and communication traffic interference on dragonfly networks equipped with burst buffers," in *Proceedings of the IEEE Cluster Conference*, ser. Cluster '17, Sep. 2017, ILNL-CONF-731482.
- [44] N. Carlini, D. Ippolito, M. Jagielski, K. Lee, F. Tramèr, and C. Zhang, "Quantifying memorization across neural language models," in *The Eleventh International Conference on Learning Representations*, 2023. [Online]. Available: https://openreview.net/forum?id=TatRHT_1cK
- [45] M. M. Grynbaum and R. Mac, "The times sues openai and microsoft over ai use of copyrighted work," *The New York Times*, vol. 27, 2023.
- [46] N. Carlini, F. Tramèr, E. Wallace, M. Jagielski, A. Herbert-Voss, K. Lee, A. Roberts, T. Brown, D. Song, U. Erlingsson *et al.*, "Extracting training data from large language models," in *30th USENIX Security Symposium (USENIX Security 21)*, 2021, pp. 2633–2650.
- [47] S. Biderman, H. Schoelkopf, Q. G. Anthony, H. Bradley, K. O'Brien, E. Hallahan, M. A. Khan, S. Purohit, U. S. Prashanth, E. Raff *et al.*, "Pythia: A suite for analyzing large language models across training and scaling," in *International Conference on Machine Learning*. PMLR, 2023, pp. 2397–2430.
- [48] P. Zhang, G. Zeng, T. Wang, and W. Lu, "Tinyllama: An open-source small language model," Tech. Rep., 2024.
- [49] A. Dubey, A. Jauhri, A. Pandey, A. Kadian, A. Al-Dahle, A. Letman, A. Mathur, A. Schelten, A. Yang, A. Fan *et al.*, "The llama 3 herd of models," Tech. Rep., 2024.
- [50] A. Hans, Y. Wen, N. Jain, J. Kirchenbauer, H. Kazemi, P. Singhanian, S. Singh, G. Somepalli, J. Geiping, A. Bhatele *et al.*, "Be like a goldfish, don't memorize! mitigating memorization in generative llms," *arXiv preprint arXiv:2406.10209*, 2024.